Optical and Quantum Electronics (2018) 50:339
https://doi.org/10.1007/s11082-018-1598-6

Effect of thickness on the optoelectronic properties of electrodeposited nanostructured SnS films

Farhad Niknia[1] · Farid Jamali-Sheini[2] · Ramin Yousefi[3] · Mohsen Cheraghizade[1]

Received: 9 November 2017 / Accepted: 13 August 2018 / Published online: 25 August 2018

Abstract
The present study focuses on the effect of film thickness on the physical properties of tin mono-sulfide (SnS) nanostructures deposited through an electrodeposition technique. The SnS films were characterized using X-ray diffraction (XRD) analysis, which confirmed the formation of polycrystalline orthorhombic SnS thin films. The crystallite size and lattice parameters were estimated from the XRD patterns. The effect of the deposition voltage on the surface morphology of the deposited films was evaluated by field emission electron microscopy (FESEM). The FESEM images revealed that the nanostructures possess plate-like and bulky pyramid morphologies. Also, optical plots of the thin films were considered, which determined the direct band gap energies of the samples as 1.42–1.50 eV. Finally, Mott–Schottky measurements indicated that the samples have *p-type* conductivity and the carrier concentrations of the SnS films improve with the increase of their thicknesses.

Keywords SnS nanostructures · Electrodeposition technique · Film thickness · Optical and electrical properties

1 Introduction

Tin mono-sulfide (SnS) is a compound semiconductor of the IV–VI group with a *p-type* nature, high absorption coefficient ($> 10^4$ cm^{-1}), 1.00–1.30 eV direct optical band gap and an orthorhombic structure (Devika et al. 2007a, b; Nwofe et al. 2012; Cheraghizade et al. 2017; Jamali-Sheini et al. 2018a, b). SnS has received much attraction due to its small band gap energy and its potential application in solar cells. Moreover, its nontoxicity, eco-friendliness, simple preparation and band gap adjustability in the range of visible light make SnS a reliable optoelectronic material (Ghosh et al. 2008; Guneri et al. 2010; Jamali-Sheini

✉ Farid Jamali-Sheini
faridjamali@iau.ahvaz.ac.ir; faridjamali2003@yahoo.com

[1] Young Researchers and Elite Club, Ahvaz Branch, Islamic Azad University, Ahvaz, Iran

[2] Advanced Surface Engineering and Nano Materials Research Center, Department of Physics, Ahvaz Branch, Islamic Azad University, Ahvaz, Iran

[3] Department of Physics, Masjed-Soleiman Branch, Islamic Azad University (I.A.U), Masjed-Soleiman, Iran

et al. 2016a, b). That is why, researches have been motivated to synthesize SnS structures for fabrication of various optoelectronic devices.

To date, thin films of SnS nanostructures have been prepared through many techniques including successive ionic adsorption and reaction (SILAR) (Ghosh et al. 2008), electrochemical deposition (Niknia et al. 2015, 2016), plasma-enhanced chemical vapor deposition (PECVD) (Sanchez-Juarez and Ortiz 2002), vacuum evaporation (Revathi et al. 2014), radio frequency (RF) sputtering (Hartman et al. 2011), dip coating (Sunil et al. 2016), chemical bath deposition (CBD) (Tanusevski 2003), chemical spray pyrolysis (Salah et al. 2005) and brush plating (Subramanian et al. 2003). In addition, numerous researches have investigated the effect of different parameters on thickness of the SnS thin films and, consequently, their structural and optical properties using different methods of film deposition. For example, Devika et al. (2007a, b), Nwofe et al. (2012) and El-Nahass et al. (2002) synthesized SnS films with various thicknesses on glass substrates through a thermal evaporation method. Devika et al. observed that the activation energy, electrical resistivity and optical band gap of the films depend on the preferred growth orientation, strongly. They stated that the increase of film thickness reduces the electrical resistivity of the films. Nwofe et al. showed that the SnS thin films with higher thicknesses present lower levels of transmittance, reflectance and absorption coefficient. They added that the refractive index and dissipation factors of SnS films decrease by the increase of film thickness. In consistence with the results of Nwofe et al., El-Nahass et al. showed that higher annealing temperatures yield thicker films with lower transmittance and reflectance.

In some other studies, e.g. the studies of the Nair group (Nair and Nair 1991) and Avellaneda et al. (2009), SnS thin films with different thicknesses were grown through chemical deposition (CD) to study the optical, electrical and photovoltaic properties of the deposited films. The group of Nair found out that increasing the time and temperature of CD causes higher film thicknesses and the films with higher thicknesses provide improved thickness-dependent photocurrent and optical and electrical conductivities due to trapping charge carriers at their surfaces and inter-grain boundaries. Avellaneda et al. reported that SnS thin films with higher thicknesses are a better choice for the absorber layers of photovoltaic cells since application of thicker SnS films promotes their open circuit voltage (V_{oc}), short circuit current (I_{sc}) and efficiency. Also, they observed that thicker SnS films increase the series resistance of photovoltaic cells and decrease the cells' shunt resistance.

In the studies of the Tanusevski and Poelman group (Tanuševski and Poelman 2003), and Hartman et al. (2011), SnS thin films with various thicknesses were grown by the electron beam evaporation, CBD and RF sputtering methods, respectively, and the effect of different factors were evaluated. Using atomic force microscopy (AFM) analysis, the Tanusevski and Poelman group understood that the root mean square (RMS) roughness of SnS films increases with film thickness. Tanusevski investigated the impact of deposition time and demonstrated that the thickness of the SnS thin films grown by the CBD technique increases linearly from 4 to 10 h and, then, saturates in the range of 10–18 h. On the other hand, Hartman et al. studied the SnS thin films that were grown at various argon pressures and powers and observed that higher argon pressures give higher film thicknesses, decrease the indirect band gap of SnS and grain length, and increase the Sn/S atomic ratio and resistivity.

Takeuchi et al. (2003) and Mishra et al. (1989) investigated the influence of thickness on the structural and optical properties of the SnS films that were deposited by electrodeposition. Takeuchi et al. employed the normal and pulsed electrodeposition methods for the growth of SnS films. They observed that the linearity of film thickness increases with deposition time. Mishra et al. found out that thicker SnS thin films contain more cracks and

flake-like morphologies, especially when rinsed with water. Forthermore, they showed that thinner films result in hillock like forms including coalescing grains and noticed that the breadth of the grains increases with film thickness. In another study, Mishra et al. reported synthesis of SnS films from a non-aqueous solution by an electrodeposition method using a standard electrolyte and studied the physical and electrical properties of the films.

Therefore, in general, the research works on SnS thin films have focused on preparing SnS films by the thermal evaporation, sputtering, E-beam evaporation, CBD methods and investigating the electro-optical behavior of the deposited films. However, in the present study, SnS films with different thicknesses are prepared via electrodeposition of an aqueous solution and the effect of thickness on the optical properties of the films is studied by calculating the derivative of the absorption spectra. In addition, the electrical behavior of the films is investigated based on their current density versus voltage (J–V), Mott–Schottky (MS) and photo-response plots to assess applicability of the films to photovoltaic devices. This study relies on electrodeposition since it is one of the easiest and cost-effective methods for deposition of thin films, particularly when a large deposition area is needed.

2 Experimental section

2.1 Synthesis

A conventional three-electrode electrochemical cell was used for synthesis of the SnS thin films while an aqueous solution including $SnCl_2$ (2×10^{-3} M) and $Na_2S_2O_3$ (20×10^{-3} M) (both high purity chemicals were purchased from Sigma-Aldrich) at pH 1.5 was applied as the electrolyte medium. The temperature of the cell was maintained at 80 °C. A fluorine-doped tin oxide (FTO) coated glass substrate, a platinum (Pt) sheet and a saturated calomel electrode (SCE, $E_0=0.244$ V vs. NHE) were employed as the working, counter and reference electrodes, respectively. Before using of the FTO substrate and the Pt electrode, they were ultrasonically cleaned for 10 min in acetone and methanol, respectively. To carry out the electrochemical evaluations, a computer-controlled electrochemical analyzer (Potentiostat, Autolab, A3ut71167, Netherlands) was used. The impacts of the film growth conditions including voltage (-0.7 and -1.2 V) as a result of reduction potential in the cyclic voltammetry (CV) plot (Fig. 1) and deposition time (30, 45, and 60 min) on the physical properties of the thin films were investigated. After each experiment, the deposited films were gently washed in water and dried in the air, naturally. The surfaces of the deposited films were dark brown and uniform. Throughout the paper, to distinguish the samples prepared using -0.7 V voltage and 30, 45 and 60 min electrodeposition time and the samples obtained by applying -1.2 V voltage and 30, 45 and 60 min time they are called Sn (0), Sn (1), Sn (2), Sn (3), Sn (4) and Sn (5), respectively.

2.2 Characterizations

The structure of the deposited films was determined using an XRD system (Philips X'Pert Pro MPD) with the Cu $K_\alpha=1.5406$ Å radiation source. The surface morphology and composition of the films were characterized by applying a FESEM (Ziess ΣIGMA VP) instrument operating at 20 kV voltage and equipped with an energy dispersive X-ray (EDX) detector. The optical properties were studied by recording the photoluminescence (PL) and UV–Vis–NIR spectra of the films at ambient temperature. For the purpose of

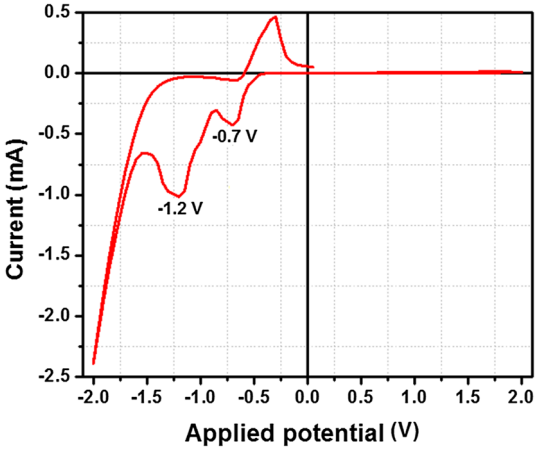

Fig. 1 CV plot for obtaining optimum deposition potential of SnS films

recording the UV–Vis–NIR diffuse reflectance spectra (DRS) over the wavelength range of 500–1200 nm, a Perkin-Elmer Lambda-950 UV–Vis–NIR spectrophotometer was used while the PL spectra were measured by a Varian-Cary Eclipse PL spectrometer. A xenon lamp with the excitation wavelength of ~ 440 nm was used as the light source.

2.3 Electrical characterizations

The optical cells were assembled using Pt foils as the counter electrodes and the films deposited on the FTO substrates as the working electrodes. Then, the electrodes were sealed in a sandwich cell and in a 100-µm-thick spacer filled with the electrolyte. The applied electrolyte solution was composed of I^-/I^{3-}. An LCR meter (LCR-8000G Series-Gwinstek) with 1 kHz frequency was used for measuring the capacitance–voltage (C–V) properties of the cells and obtaining their MS plots. The potentiostat was also employed to plot the J–V curves. In this respect, a 100 W xenon lamp was adopted as the light source and the light intensity was calibrated considering a standard silicon solar cell. The effective area of the samples that was exposed to the light rays was 0.5 cm^2 and the distance between the lamp and the working electrode was fixed at 20 cm. To explore the photocurrent properties, photocurrent measurement was carried out by a solar simulator (Solar cell simulator IIIS-200+, Nanosat Co., Iran) with 100 mW/cm^2 illumination intensity (1.5 Air Mass). It should be noted that the generated photocurrent was continuously recorded during both irradiation and darkness periods. All experiments were performed under ambient conditions.

3 Results and discussion

The XRD patterns of the films deposited onto the FTO substrates using various deposition times and voltages are shown in Fig. 2. As Fig. 2 displays, the XRD patterns contain several peaks, which indicate that the deposited films have polycrystalline orthorhombic structures. To be more specific, the XRD patterns represent different planes that are consistent with the 01-079-2193, 01-075-0925 and 00-039-0354 JCPDS card numbers (ICDD 1997).

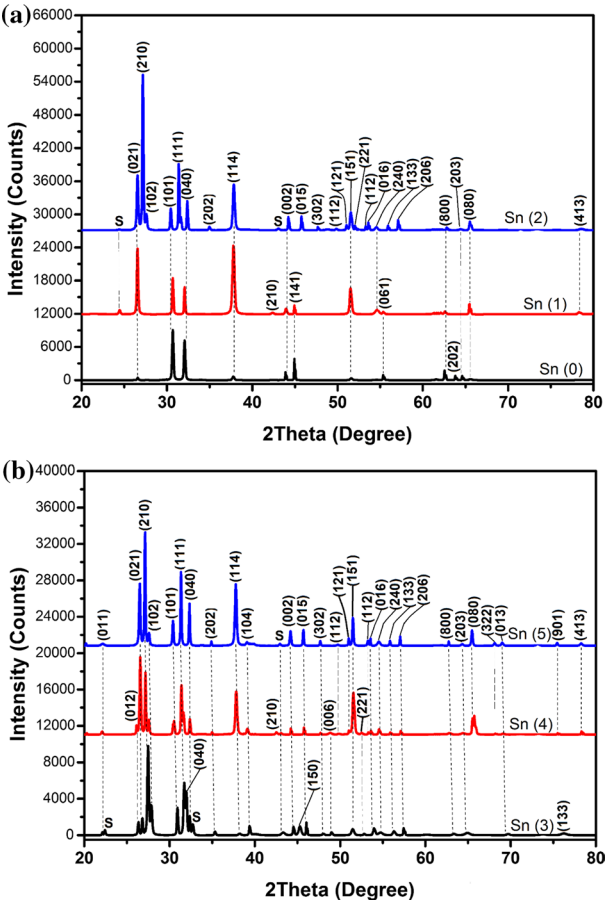

Fig. 2 XRD patterns of the nanostructured SnS thin films at different deposition times (30, 45 and 60 min) and voltages: **a** − 0.7 V, and **b** − 1.2 V

The lattice parameters (a, b, and c) of the synthesized films were calculated using Eq. (1) that is consisted of the inter-planar spacing (*d*) of the crystal planes in orthorhombic structures and Miller indices (*hkl*) (Cullity and Stock 2013).

$$\frac{1}{d^2} = \frac{h^2}{a^2} + \frac{k^2}{b^2} + \frac{l^2}{c^2} \tag{1}$$

The lattice parameters of the Sn (0) sample were determined as $a = 4.35$ Å, $b = 11.22$ Å and $c = 3.95$ Å with $a/c = 1.10$, which indicate a good consistency with the standard values of the JCPDS dataset. Moreover, using of the Scherrer's equation (Jamali-Sheini et al. 2015) revealed that the average SnS crystallite sizes of the Sn (0), Sn (1), Sn (2), Sn (3), Sn (4) and Sn (5) films are 47, 55, 64, 51, 55, and 74 nm, respectively. Therefore, increasing the deposition time increases the crystallite size from 48 to 66 nm, at − 0.7 eV, and from 49 to 75 nm, at − 1.2 eV. This variation in the average crystallite sizes can be due to the changes induced in the crystal growth and nucleation processes by varying the deposition time and voltage. This inhibits the growth of the deposited atoms through partial restriction

of their mobility and reduces the crystallite size of the SnS films deposited with lower thicknesses.

In addition to evaluating the crystal structures of the deposited films, their surface morphology was studied. The results are displayed in Fig. 3. As Fig. 3 unravels, the prepared SnS films contain edged and faceted particles. At the voltage of − 0.7 V and 30 min deposition time (Sn (0)), plate-like structures with two different sizes can be observed. Meantime, the concentration of the smaller plate-like structures increases with the deposition time at − 0.7 voltage, i.e. Sn (1) and Sn (2). Also, in the case of the − 1.2 V deposition voltage and 30 min deposition time (Sn (3)), two types of morphology can be seen including bulky pyramid and small plate-like structures. Similar to the case of the − 0.7 voltage, increase of the deposition time increases the size of the deposited structures, i.e. Sn (4) and Sn (5). Also, according to the cross section FESEM images that are inset into each image and the measured thicknesses (Table 1), thickness of the deposited films increases with deposition time. Therefore, longer electrodeposition processes provide larger crystallite sizes and thicker films.

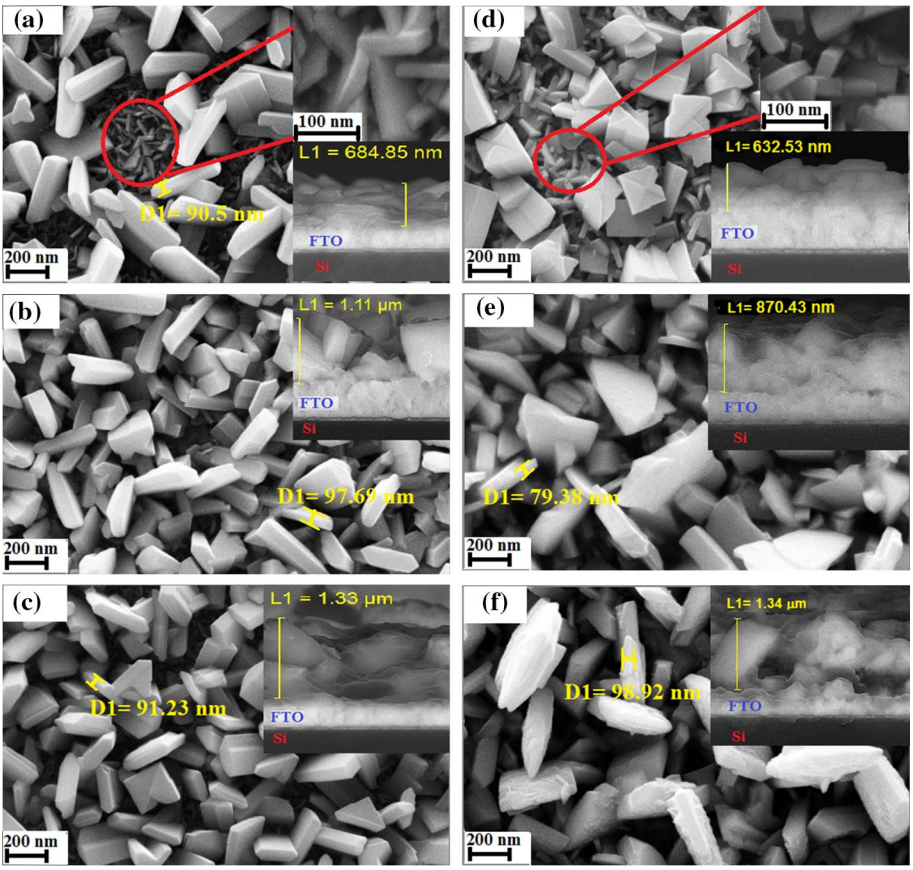

Fig. 3 FESEM images of the **a** Sn (0), **b** Sn (1), **c** Sn (2), **d** Sn (3), **e** Sn (4), and **f** Sn (5) thin films grown on the FTO substrates. The insets show their cross FESEM images

Table 1 Deposition conditions of the SnS films

Samples	Voltage (V)	Tim (min)	Thickness (μm)
Sn (0)	− 0.7	30	0.68
Sn (1)	− 0.7	45	1.11
Sn (2)	− 0.7	60	1.33
Sn (3)	− 1.2	30	0.63
Sn (4)	− 1.2	45	0.87
Sn (5)	− 1.2	60	1.34

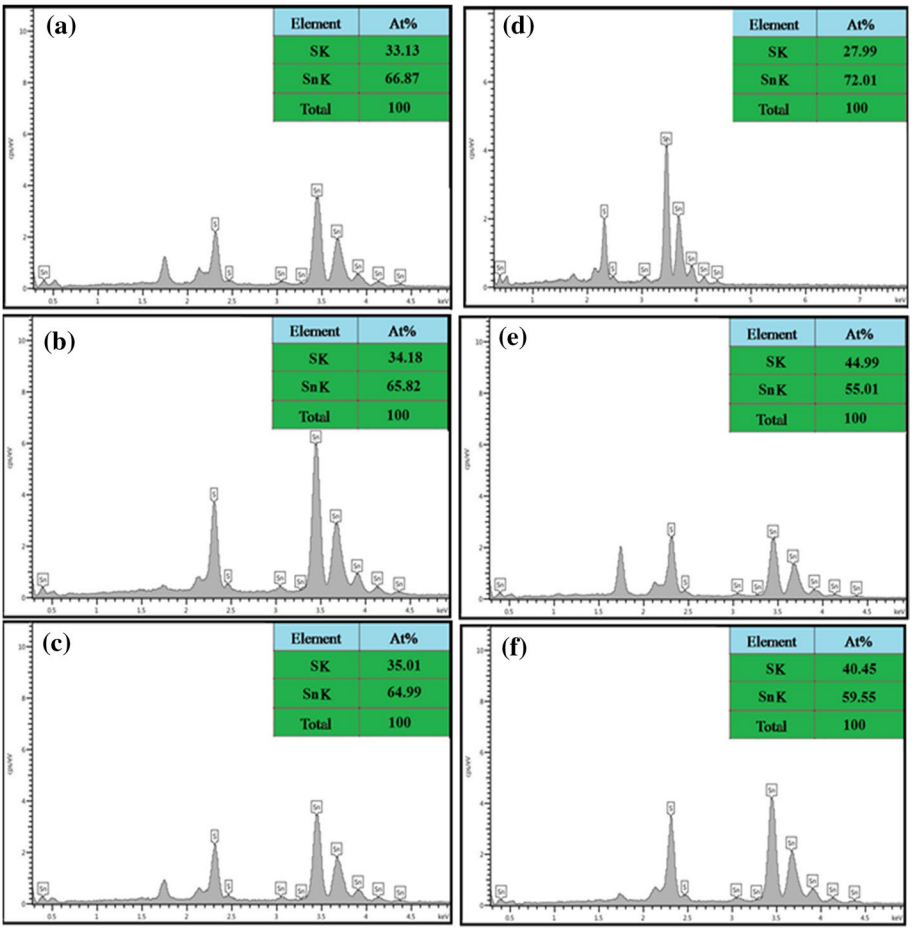

Fig. 4 EDX analysis of the **a** Sn (0), **b** Sn (1), **c** Sn (2), **d** Sn (3), **e** Sn (4), and **f** Sn (5) thin films

The EDX-based elemental analysis results of the nanostructured SnS films synthesized at various conditions are exhibited in Fig. 4, which supports the existence of the Sn and S elements in the films and reports their atomic percentage (At%) values. With respect to Fig. 4, prolonging the deposition process increases the percentage of the S atom in the

films. So that, stoichiometric SnS thin films can be obtained by depositing thicker films. It means that increasing the thickness of the film can give a SnS layer with stoichiometric structures. Such finding has been also reported by Sinsermsuksakul et al., who grow SnS thin films with different thicknesses using an atomic layer deposition (ALD) technique (Sinsermsuksakul et al. 2011).

Figure 5 presents the PL emission spectra of the nanostructured SnS films. As it can be observed, the nanostructured SnS films of outline two strong emission bands centered at 470 nm (blue emission) and 530 nm (green emission). Meanwhile, the band-to-band emission of the SnS nanostructures is positioned around 825 nm and corresponds to a 1.51 eV energy gap. The strong blue and green emission bands are like that of SnS nanoparticles and are related to the influence of crystal defects (El-Nahass et al. 2002; Devika et al. 2007a, b; Nwofe et al. 2012). In other words, the observed transitions and peaks can be attributed to the existence of oxygen and different kinds of defects including interstitials and stacking faults (Yue et al. 2009, 2012; Kumar et al. 2014). On the other hand, the PL spectra illustrate that increasing film thickness results in a red shift and reduces the intensity of the PL emission bands of the SnS thin films. This red shift is accompanied with a decrease in the energy band gaps of the thicker SnS films. The difference in the PL features of the SnS films is a result of a combined set of factors, such as their various compositions, sizes/effective surface areas, band gaps, morphologies, crystallinities and crystal defects. Since almost all these factors are strongly coupled, it is hard to characterize a specific function about the influence of a single parameter on the PL results.

The UV–Vis–NIR absorption spectra of the SnS films at room temperature are shown in Fig. 6. According to the spectra, all SnS samples produced under various conditions give similar characteristic absorption peaks. The obtained spectra were used to determine the optical band gap energies of the films. In this respect, the direct band gap could be predicted as either the maximum of the first derivative of the absorbance plot versus energy or the point that the second derivative curve intersects with the energy axis from the confluence of the peak and valley with the highest intensity (Yousefi et al. 2014). In this study, the second derivatives were studied (Fig. 7). It was seen that the band gap value decreases with the increase of thickness, in harmony with the PL results and the results obtained by Bashkirov et al., who deposited different SnS thin films using a hot wall deposition technique (Bashkirov et al. 2011). Lastly, by changing the thickness of deposited films the sequence variation in the physical

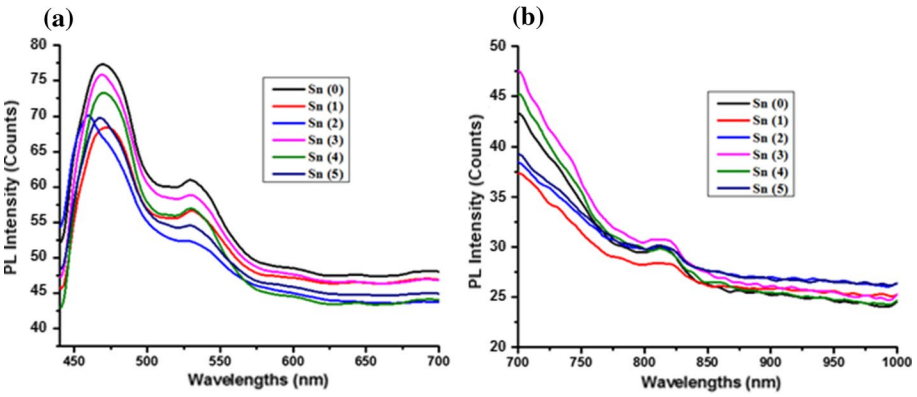

Fig. 5 PL spectra of the nanostructured SnS thin films at **a** visible, and **b** near infrared regions

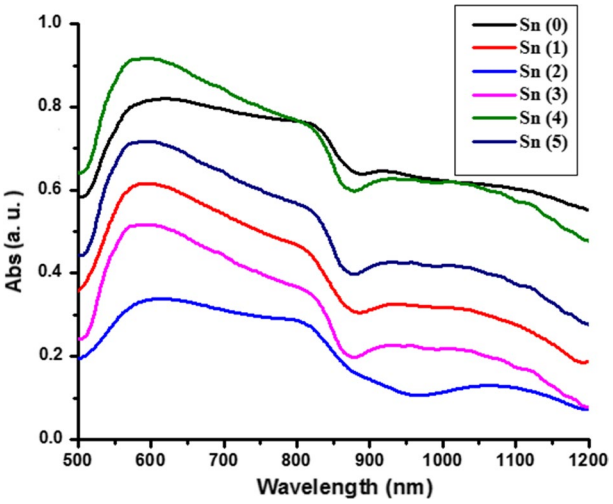

Fig. 6 UV–Vis–NIR absorption spectra of the nanostructured SnS thin films

property was expected but difference in the optical property (absorption values and the intensity of PL emission) of the films are a result of the combined action of many factors such as their atomic compositions, sizes/effective surface areas of crystalline, crystallinity, and crystal defects. As almost all of the aforementioned factors are strongly coupled, it is hard to characterize the specific function in the optical property of deposited SnS films.

To determine the nature of the semiconductor films and the relevant parameters, the capacitance versus potentials of the SnS thin films deposited with different thicknesses on the FTO substrates were measured in the thickness ranges of 0.63–1.34 µm. Then, the MS plots of the films applied in the system of FTO/SnS/iodide/Pt were obtained by considering the MS equation for non-intrinsic semiconductors (Eq. (2)) (Jamali-Sheini et al. 2016a, b).

$$\frac{1}{C_{scl}^2} = \frac{-2}{e \times \varepsilon_0 \times \varepsilon_s \times N_A}\left(V - V_{fb} - \frac{kT}{e}\right) \tag{2}$$

In Eq. (2), C_{scl} is the capacitance of the space charge layer, e is the electron charge, ε_0 refers to the free space permittivity, ε_s stands for the semiconductor static permittivity, N_A is concentration of the acceptor, V is the applied voltage, V_{fb} is denoted to the potential of flat band, k is the Boltzmann constant and T (K) is the temperature. It should be noted that Eq. (2) is just true for the depletion layers that can be considered as a space charge region, where majority of the carrier density is depleted in comparison with the bulk density. Figure 8 shows the typical MS plots achieved for different voltages. The negative slopes of the MS plots verifies the *p-type* conductivity of the nanostructured films, as expected due to the presence of intrinsic Sn deficiency in stoichiometric SnS structure that create acceptor levels (Subramanian et al. 2001). Besides determining the conductivity type of the films, the intercepts of the linear plots at $1/C^2 = 0$ were concerned to give the junction flat band potentials of the films. The obtained flat band potentials were found to be accurate for the given carrier concentrations, electrolytes and majority carrier types. Moreover, the acceptor concentration (N_A) of the films was determined from the slope of their MS plots by using Eq. (3) (Chen et al. 2016) and taking the required ε_s and ε_0 values from the literature (Haynes 2012).

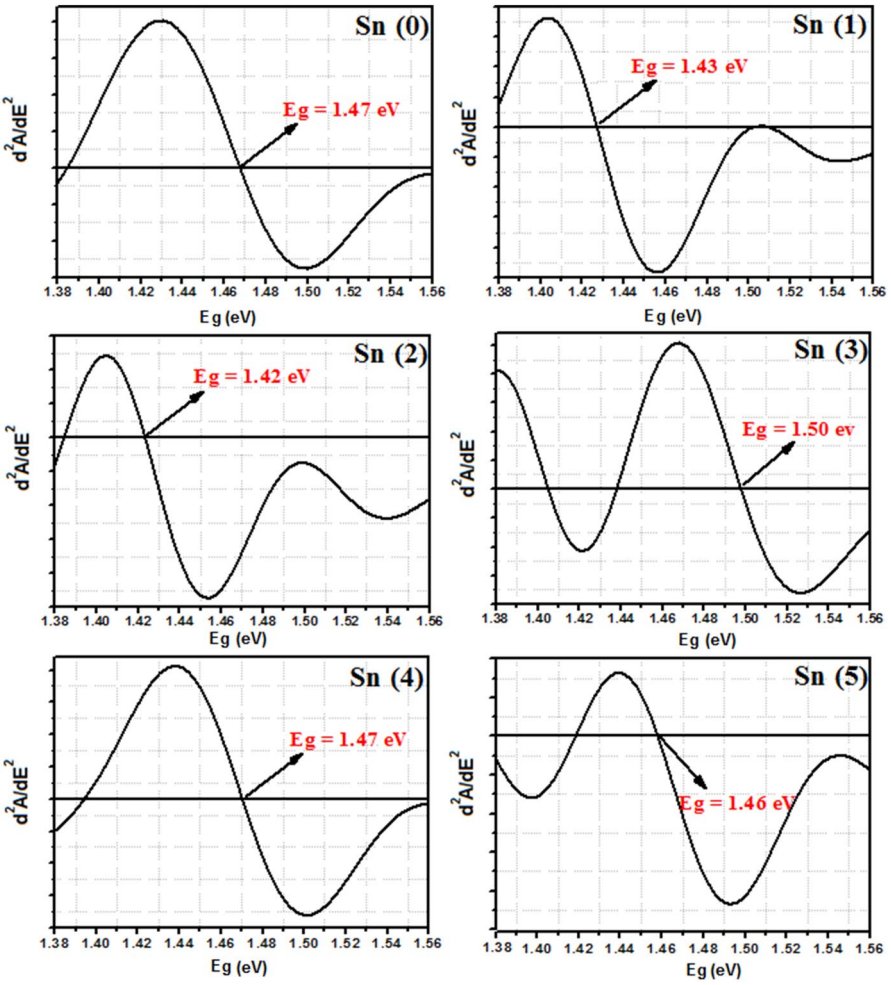

Fig. 7 Derivatives of the UV–Vis–NIR absorption spectra of the nanostructured SnS thin films

$$N_A = \frac{2}{\varepsilon_s \times \varepsilon_0 \times e \times Slope} \tag{3}$$

The calculated acceptor concentrations, as well as the other physical parameters, are reported in Table 2. Based on Table 2, thicker films have higher acceptor concentrations in contrast with the EDX results shown in Fig. 4, which indicated lower Sn At% for thicker films and, therefore, higher acceptor levels. Furthermore, the obtained carrier concentrations are relatively lower than those usually encountered in the literature, which can be originated from different factors including ionized impurities, natural impurities, different defects, dislocations and grain boundaries. In fact, due to the small grain size of the SnS thin films, the carriers have to travel multiple grain boundaries that results in a low carrier concentration (Hegde et al. 2013).

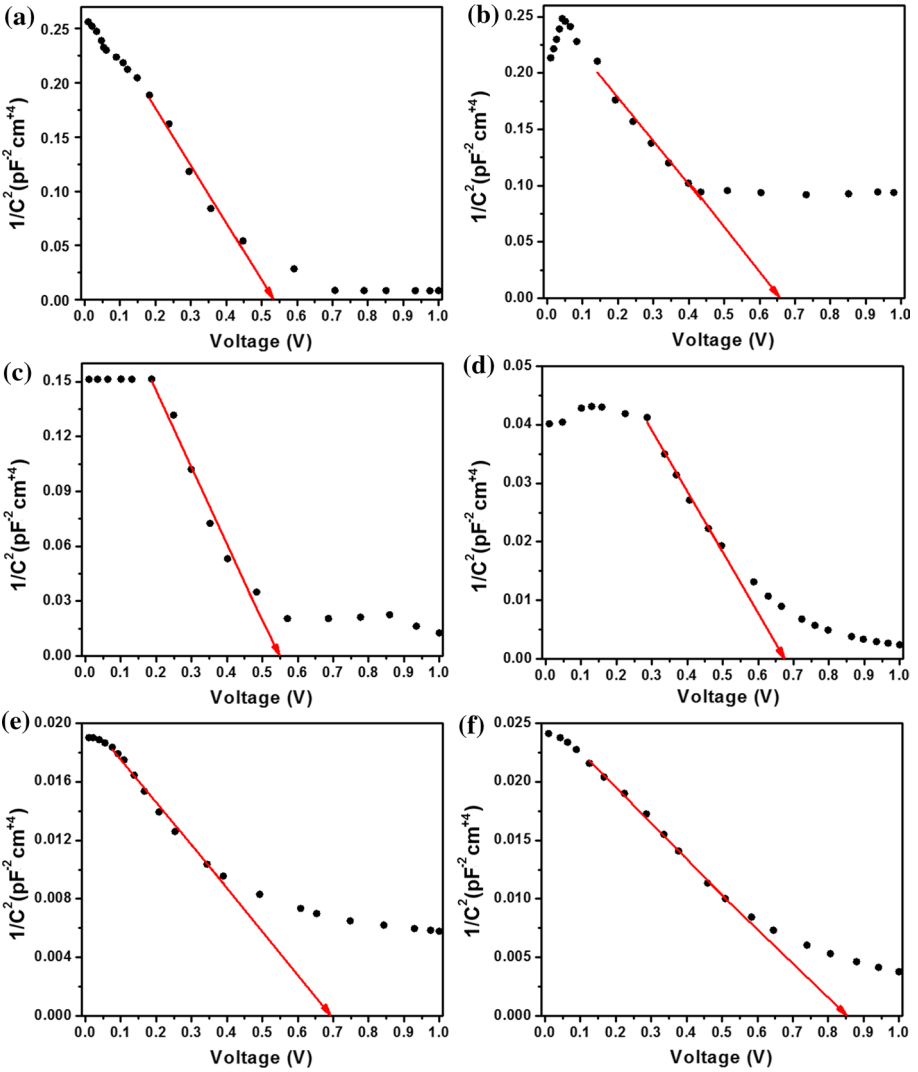

Fig. 8 The MS plots of the **a** Sn (0), **b** Sn (1), **c** Sn (2), **d** Sn (3), **e** Sn (4), and **f** Sn (5) nanostructured SnS thin films, at 1 kHz frequency

Table 2 The physical parameters obtained from the MS plots of the SnS thin films

Physical parameters/samples	Sn (0)	Sn (1)	Sn (2)	Sn (3)	Sn (4)	Sn (5)
Conductivity	*p*	*p*	*p*	*p*	*p*	*p*
Flat band voltage (V)	0.53	0.66	0.62	0.67	0.70	0.85
Acceptor concentration (10^{+15}/cm^3)	0.09	0.13	0.12	0.48	1.71	1.62

The J–V curves of the fabricated devices with 0.68, 1.11 and 1.33 µm film thicknesses were recorded by gate voltage sweeping from −3 to 3 V. According to the J–V curves in Fig. 9a, b, increasing the thickness leads to the change of current density. Also, the current density of the samples deposited at −1.2 V are higher at more positive bias potentials, which demonstrates that the SnS films are composed of *p-type* phases, majorly and not completely. The loss of some *p-type* phases might be due to the loss of Sn during the prolonged deposition processes. In agreement with this finding, some earlier studies have shown that S-rich SnS films contain both *n*-and *p-type* phases (Sajeesh et al. 2010).

In the next step, the current density profile of the device was determined as a function of time under the illumination and darkness conditions (Figs. 9c, d). Based on the obtained curves, it is clear that the current density of the device reduces upon illumination. Such behavior is associated with cathodic photocurrents and is a characteristic of *p-type* semiconductors (Ghanbari et al. 2018; Jamali-Sheini et al. 2018a, b), in agreement with the pervious results (the MS plot). The maximum current density after exposing the device to light is related to the thickest SnS film, i.e. Sn (5), and is about 38 nA/cm^2. This value might be compared with the current density of Sn (3) (15 nA/cm^2) with a lower thickness. Increase of the photocurrent density with thickness can be related to the increase of carrier concentration, with respect to the MS results. Similarly, a higher electron-to-photon conversion with the increase of SnS film thickness is reported by Avellaneda et al. (2009).

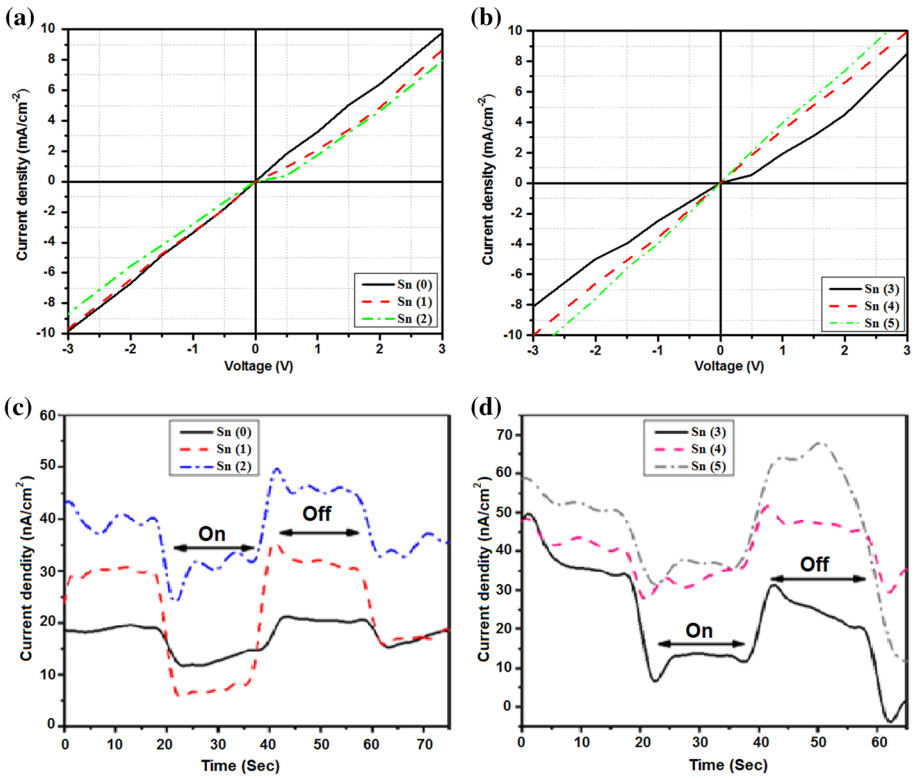

Fig. 9 **a**, **b** J–V curves of the nanostructured SnS thin films under darkness, and **c**, **d** the typical photocurrent response of the nanostructured SnS thin films under pulsed illumination by the Xenon light (0 V bias)

At last, reproducibly of the measured photocurrent response was investigated by turning the solar simulator ON and OFF, periodically. Switching from the darkness to illumination condition was observed to increase the current of the SnS film to a stable value within a short time.

4 Conclusion

In this study, *p-type* SnS thin films were successfully synthesized using an electrodeposition technique. The electrochemical system was a three-electrode cell with a FTO substrate, as the working electrode. All deposited SnS films contained a single orthorhombic phase. Increasing the deposition time increased the thickness and uniformity of the SnS films, significantly. The optical band gap of the as-deposited films ranged from 1.42 to 1.50 eV. Finally, using of greater film thicknesses resulted in higher photocurrent densities and provided more electrical contact points in the SnS films.

Acknowledgements F. Jamali-Sheini and R. Yousefi gratefully acknowledge Islamic Azad University, the Ahvaz and Masjed-Soleiman Branches, respectively, for their financial support of this research work. F. Jamali-Sheini also appreciates Advanced Surface Engineering and Nano Materials Research Center, Ahvaz Branch, Islamic Azad University, Ahvaz, Iran, for instrumentational support.

References

Avellaneda, D., Nair, M.T.S., Nair, P.K.: Photovoltaic structures using chemically deposited tin sulfide thin films. Thin Solid Films **517**(7), 2500–2502 (2009)

Bashkirov, S.A., Gremenok, V.F., Ivanov, V.A.: Physical properties of SnS thin films fabricated by hot wall deposition. Semiconductors **45**(6), 749–752 (2011)

Chen, H.-J., Fu, S.-W., Wu, S.-H., Tsai, T.-C., Wu, H.-T., Shih, C.-F.: Impact of SnS buffer layer at Mo/Cu_2ZnSnS_4 interface. J. Am. Ceram. Soc. **99**(5), 1808–1814 (2016)

Cheraghizade, M., Jamali-Sheini, F., Yousefi, R., Niknia, F., Mahmoudian, M.R., Sookhakian, M.: The effect of tin sulfide quantum dots size on photocatalytic and photovoltaic performance. Mater. Chem. Phys. **195**, 187–194 (2017)

Cullity, B.D., Stock, S.R.: Elements of X-ray Diffraction. Pearson, London (2013)

Devika, M., Reddy, N.K., Ramesh, K., Ganesan, R., Gunasekhar, K.R., Gopal, E.S.R., Reddy, K.T.R.: Thickness effect on the physical properties of evaporated SnS films. J. Electrochem. Soc. **154**(2), H67–H73 (2007a)

Devika, M., Reddy, N.K., Reddy, D.S., Reddy, S.V., Ramesh, K., Gopal, E.S.R., Gunasekhar, K.R., Ganesan, V., Hahn, Y.B.: Optimization of the distance between source and substrate for device-grade SnS films grown by the thermal evaporation technique. J. Phys.: Condens. Matter **19**(30), 306003 (2007b)

El-Nahass, M.M., Zeyada, H.M., Aziz, M.S., El-Ghamaz, N.A.: Optical properties of thermally evaporated SnS thin films. Opt. Mater. **20**(3), 159–170 (2002)

Ghanbari, B., Jamali-Sheini, F., Yousefi, R.: Microwave-assisted solvothermal synthesis and optoelectronic properties of γ-MnS nanoparticles. J. Mater. Sci.: Mater. Electron. **29**(13), 10976–10985 (2018)

Ghosh, B., Das, M., Banerjee, P., Das, S.: Fabrication and optical properties of SnS thin films by SILAR method. Appl. Surf. Sci. **254**(20), 6436–6440 (2008)

Guneri, E., Ulutas, C., Kirmizigul, F., Altindemir, G., Gode, F., Gumus, C.: Effect of deposition time on structural, electrical, and optical properties of SnS thin films deposited by chemical bath deposition. Appl. Surf. Sci. **257**(4), 1189–1195 (2010)

Hartman, K., Johnson, J.L., Bertoni, M.I., Recht, D., Aziz, M.J., Scarpulla, M.A., Buonassisi, T.: SnS thin-films by RF sputtering at room temperature. Thin Solid Films **519**(21), 7421–7424 (2011)

Haynes, W.M.: CRC Handbook of Chemistry and Physics, 93rd edn. Taylor & Francis, Routledge (2012)

Hegde, S.S., Kunjomana, A.G., Prashantha, M., Kumar, C., Ramesh, K.: Photovoltaic structures using thermally evaporated SnS and CdS thin films. Thin Solid Films **545**, 543–547 (2013)

ICDD, P.D.F.: International Centre for Diffraction Data. Powder Diffraction File, Newtown Square, Pennsylvania, USA (1997)
Jamali-Sheini, F., Yousefi, R., Bakr, N.A., Cheraghizade, M., Sookhakian, M., Huang, N.M.: Highly efficient photo-degradation of methyl blue and band gap shift of SnS nanoparticles under different sonication frequencies. Mater. Sci. Semicond. Process. **32**, 172–178 (2015)
Jamali-Sheini, F., Cheraghizade, M., Niknia, F., Yousefi, R.: Enhanced photovoltaic performance of tin sulfide nanoparticles by indium doping. MRS Commun. **6**(4), 421–428 (2016a)
Jamali-Sheini, F., Cheraghizade, M., Yousefi, R.: SnS nanosheet films deposited via thermal evaporation: the effects of buffer layers on photovoltaic performance. Solar Energy Mater. Solar Cells **154**, 49–56 (2016b)
Jamali-Sheini, F., Cheraghizade, M., Yousefi, R.: Electrochemically synthesis and optoelectronic properties of Pb- and Zn-doped nanostructured SnSe films. Appl. Surf. Sci. **443**, 345–353 (2018a)
Jamali-Sheini, F., Cheraghizade, M., Yousefi, R.: Ultrasonic synthesis of In-doped SnS nanoparticles and their physical properties. Solid State Sci. **79**, 30–37 (2018b)
Kumar, K.S., Manoharan, C., Dhanapandian, S., Manohari, A.G., Mahalingam, T.: Effect of indium incorporation on properties of SnS thin films prepared by spray pyrolysis. Optik-Int. J. Light Electron. Opt. **125**(15), 3996–4000 (2014)
Mishra, K., Rajeshwar, K., Weiss, A., Murley, M., Engelken, R.D., Slayton, M., McCloud, H.E.: Electrodeposition and characterization of SnS thin films. J. Electrochem. Soc. **136**(7), 1915–1923 (1989)
Nair, M.T.S., Nair, P.K.: Simplified chemical deposition technique for good quality SnS thin films. Semicond. Sci. Technol. **6**(2), 132 (1991)
Niknia, F., Jamali-Sheini, F., Yousefi, R.: Photocurrent properties of undoped and Pb-doped SnS nanostructures grown using electrodeposition method. J. Electron. Mater. **44**(12), 4734–4739 (2015)
Niknia, F., Jamali-Sheini, F., Yousefi, R.: Examining the effect of Zn dopant on physical properties of nanostructured SnS thin film by using electrodeposition. J. Appl. Electrochem. **46**(3), 323–330 (2016)
Nwofe, P.A., Reddy, K.T.R., Tan, J.K., Forbes, I., Miles, R.W.: Thickness dependent optical properties of thermally evaporated SnS thin films. Phys. Proced. **25**, 150–157 (2012)
Revathi, N., Bereznev, S., Loorits, M., Raudoja, J., Lehner, J., Gurevits, J., Traksmaa, R., Mikli, V., Mellikov, E., Volobujeva, O.: Annealing effect for SnS thin films prepared by high-vacuum evaporation. J. Vac. Sci. Technol., A **32**(6), 061506 (2014)
Sajeesh, T.H., Warrier, A.R., Kartha, C.S., Vijayakumar, K.P.: Optimization of parameters of chemical spray pyrolysis technique to get n and p-type layers of SnS. Thin Solid Films **518**(15), 4370–4374 (2010)
Salah, H.B.H., Bouzouita, H., Rezig, B.: Preparation and characterization of tin sulphide thin films by a spray pyrolysis technique. Thin Solid Films **480**, 439–442 (2005)
Sanchez-Juarez, A., Ortiz, A.: Effects of precursor concentration on the optical and electrical properties of Sn_XS_Y thin films prepared by plasma-enhanced chemical vapour deposition. Semicond. Sci. Technol. **17**(9), 931 (2002)
Sinsermsuksakul, P., Heo, J., Noh, W., Hock, A.S., Gordon, R.G.: Atomic layer deposition of tin monosulfide thin films. Adv. Energy Mater. **1**(6), 1116–1125 (2011)
Subramanian, B., Sanjeeviraja, C., Jayachandran, M.: Cathodic electrodeposition and analysis of SnS films for photoelectrochemical cells. Mater. Chem. Phys. **71**(1), 40–46 (2001)
Subramanian, B., Sanjeeviraja, C., Jayachandran, M.: Photoelectrochemical characteristics of brush plated tin sulfide thin films. Solar Energy Mater. Solar Cells **79**(1), 57–65 (2003)
Sunil, H.C., Mahesh, D.C., Deshpande, M.P.: SnS thin films deposited by chemical bath deposition, dip coating and SILAR techniques. J. Semicond. **37**(5), 053001 (2016)
Takeuchi, K., Ichimura, M., Arai, E., Yamazaki, Y.: SnS thin films fabricated by pulsed and normal electrochemical deposition. Solar Energy Mater. Solar Cells **75**(3), 427–432 (2003)
Tanusevski, A.: Optical and photoelectric properties of SnS thin films prepared by chemical bath deposition. Semicond. Sci. Technol. **18**(6), 501 (2003)
Tanuševski, A., Poelman, D.: Optical and photoconductive properties of SnS thin films prepared by electron beam evaporation. Solar Energy Mater. Solar Cells **80**(3), 297–303 (2003)
Yousefi, R., Cheraghizade, M., Jamali-Sheini, F., Mahmoudian, M.R., Saaédi, A., Huang, N.M.: Influences of anionic and cationic dopants on the morphology and optical properties of PbS nanostructures. Chin. Phys. B **23**(10), 108101 (2014)
Yue, G.H., Wang, W., Wang, L.S., Wang, X., Yan, P.X., Chen, Y., Peng, D.L.: The effect of anneal temperature on physical properties of SnS films. J. Alloys Compd. **474**(1), 445–449 (2009)
Yue, G.H., Lin, Y.D., Wen, X., Wang, L.S., Chen, Y.Z., Peng, D.L.: Synthesis and characterization of the SnS nanowires via chemical vapor deposition. Appl. Phys. A **106**(1), 87–91 (2012)